Effects of Sampling on Stability and Performance of Electronically Controlled Pressure-Reducing Valves

Tomasz Janus[1] and Bogumil Ulanicki[2]

Abstract: This paper explains and demonstrates how increasing a sampling period in pressure control may worsen a system's performance and lead to instability. The notion of stability of continuous-time and discrete-time systems is briefly introduced and applied to a simple closed-loop inertial system. It is then demonstrated how the stability of dynamic systems depends on a sampling period as well as on gain. Subsequently, the analysis is applied to a model of an electronically controlled pressure-reducing valve (PRV) coupled with a transient model of a water distribution network (WDN). The occurrence of instabilities at overly long sampling periods is demonstrated. Practical recommendations on the appropriate choice of sampling times are put forth based on simulation results and control engineering rules of thumb given the closed-loop system's dynamics. Performance of a theoretical pressure control scheme is then simulated under time-varying demands and with controllers designed to work at different sampling frequencies. **DOI: 10.1061/(ASCE)WR.1943-5452.0001328.**

Introduction

Pressure control is an important task in the management of water distribution networks (WDNs) and has two main functions: (1) servo control, which tracks time-varying pressure setpoints in a given node of a network in order to, e.g., minimize leakage; and (2) regulation control, which maintains the pressure setpoint irrespective of disturbances, e.g., sudden demand changes in the network or events such as pump or valve switching, hydrant opening or bursts. These two functions impose somewhat different requirements on the dynamics of the pressure control system and are be discussed in detail in this paper.

So far, most of the publications on real-time control (RTC) in WDNs have considered pressure management for leakage control and demand supply, while disturbance rejection was covered only in a handful of papers (e.g., Creaco et al. 2017, 2018). Excessive pressure in a WDN leads to elevated levels of pressure-dependent background leakage (Vicente et al. 2016) and increases the risk of bursts (Thornton and Lambert 2010). On the other hand, insufficient pressure in parts of the network may result in a reduction or a complete loss of service to some consumers. Pressure control in WDNs is most often accomplished via pressure-reducing valves (PRVs), which are usually installed at inlets to district metering areas (DMAs) and are designed to maintain the desired outlet pressure. The pressure setpoint can either be constant or follow a time trajectory, which can either be scheduled or calculated online in an outer control loop, as in, e.g., Fontana et al. (2018). Because water demands in a network follow a diurnal pattern, pressures in the network vary accordingly.

Background leakage depends on slowly varying pressure trends in the network, and hence, the speed of a servo controller can be relaxed. Consequently, the times between consecutive control actions can be in a range of minutes, provided that the controller is designed appropriately, as discussed in this paper. For constant inlet pressure, the pressures further along in the network are higher during low-demand periods and lower during high-demand periods. This may be undesirable if the aim is to keep pressures within a DMA at quasi-constant, near-optimal levels. One solution to this problem is to modulate the PRV setpoint as a function of flow, as was done by AbdelMeguid et al. (2011), using a special hydraulic device installed in a bypass circuit of a hydraulically operated PRV. Another solution is to manipulate the PRVs based on pressure measurements from within the network using electronic controllers. This was proposed in a number of publications; see Creaco et al. (2019) for a detailed review of the work in this field. In the case of hydraulic PRVs, the manipulated variable is the pressure setpoint adjusted by the pilot valve screw, which fulfills the servo control function, while the inner hydraulic circuit via the pilot valve performs a regulatory function, i.e., disturbance rejection.

Recently, some water companies have been introducing pressure control schemes where valve elements are actuated directly in feedback control loops with electronic controllers combined with electromechanical actuators. Here, these valves are called remotely controlled valves (RCVs). RCVs belong to the class of PRVs. In such valves, which are usually installed in strategic supply points in a WDN, both servo control and regulatory control are implemented using electronic control circuits. For disturbance rejection, in contrast to servo control, regulators need to react to inputs of high frequencies resulting from, e.g., sudden changes in demand, e.g., hydrant openings or valve and pump switching, which in turn necessitates short time steps between consecutive control actions. These disturbances need to be rejected because, even though they may be short-lived and, thus, have only a small impact on background leakage, they can be detrimental to WDN infrastructure and water quality. Pressure transients put strain on pipes and may cause new bursts (Malppan and Sumam 2015; Rezaei et al. 2015). They may also lead to deterioration in water quality by dislodging materials deposited on pipe walls, e.g., biofilms (Jones et al. 2015). In this solution, an appropriate choice of sampling

[1]Research Associate, Dept. of Mechanical, Aerospace, and Civil Engineering, Univ. of Manchester, George Begg Bldg., Manchester M1 3BB, UK (corresponding author). Email: tomasz.janus@manchester.ac.uk

[2]Professor Emeritus of Engineering Systems, Water Software Systems, School of Engineering and Sustainable Development, De Montfort Univ., The Gateway, Leicester LE1 9BH, UK. ORCID: https://orcid.org/0000-0002-8288-9928

Note. This manuscript was submitted on November 19, 2019; approved on September 9, 2020; published online on January 13, 2021. Discussion period open until June 13, 2021; separate discussions must be submitted for individual papers. This paper is part of the ***Journal of Water Resources Planning and Management***, © ASCE, ISSN 0733-9496.

times for both control loops becomes a legitimate engineering concern, which the authors aim to address in this paper. Moreover, the issue of appropriate selection of sampling times in digital control systems is not only restricted to PRVs but applies to other applications, including pump speed control.

The literature on the RTC of WDNs is abundant and has recently been reviewed and summarized by Creaco et al. (2019). The bulk of the publications on this topic are often based on static network models (Campisano et al. 2010, 2012; Creaco and Franchini 2013; Campisano et al. 2016; Giustolisi et al. 2017; Page et al. 2017a, b; Creaco 2017; Page et al. 2018; Berardi et al. 2018; Page and Creaco 2019). The authors investigated reductions in leakage using different control strategies and controllers within an extended-period simulation (EPS) environment where the implemented control algorithms would adjust the valve setting in between successive steady-state solutions. Since the focus was placed on water savings resulting from RTC and not on pressure control on shorter time scales characteristic of disturbances, the authors of the cited papers used long control time steps, which necessitated using small gains (i.e., slow control action) in order to maintain stability, as explained subsequently in this paper. Specifically, time steps of 3 min in, e.g., Campisano et al. (2012) and 5 min in, e.g., Giustolisi et al. (2017) were the most frequently chosen values. The dynamic behavior of the network was not considered; it was instead assumed that the chosen control time step would be sufficiently long so that the transients resulting from the valve adjustments would fade away between successive control actions. While the previously cited papers provide insight into potential water savings resulting from RTC, removal of the time dimension from the hydraulic models and, thus, of inertial (rigid-column) and wave (water hammer) dynamics did not allow the authors to investigate how the proposed control schemes would behave under time-varying demands on shorter time scales. Although it was claimed that the controller was proportional, it is in fact a discrete integral controller since its form, $\Delta a_i = K_p \Delta h_i$, implies that the control signal $a = K_p \sum_i \Delta h_i$, i.e., is proportional to the sum of the errors over the previous time steps, not the current value of the error, as in proportional controllers. As discussed subsequently, the choice of sampling times in a range of minutes required the use of rather small gain values in order to reduce the bandwidth and maintain appropriate stability margins. The proposed control schemes were designed for the purpose of responding to low-frequency pressure signal components for leakage management. They are unable to respond to higher-frequency signals resulting from demand changes, which require controllers with larger bandwidths, i.e., higher gain values and correspondingly shorter sampling periods. As demonstrated, the stability of discrete-time closed-loop systems depends on the dynamics of the open-loop system (without feedback) and, for a given system and a given controller, is a function of the open-loop static gain (denoted by K), as well as the sampling period T.

Recently, some authors have discussed implementations of the aforementioned control algorithms using transient WDN simulation models and analyzed their performances at different control time steps. Using a form of a valve model–derived control algorithm from Creaco and Franchini (2013), Creaco et al. (2017) reported a stable control system at time steps $\Delta t = 180$ s and longer but oscillatory behavior at $\Delta t = 3$ s. The authors concluded that $\Delta t = 180$ s was a good choice for a control interval. However, the proposed control system was tested only during a time period when demand was relatively constant, and thus its disturbance rejection properties could not be assessed. Creaco et al. (2018), using control time steps $\Delta t = 1$ min and 3 min in combination with a transient hydraulic model, noted an improvement with a smaller time step out of the two but then concluded that if the control time were overly reduced, control instabilities could arise. The authors tested the dynamic response of their remotely controlled valve to the activation of a hydrant, but, owing to a long control time step and small gain warranting stability in that particular case, the system was unable to maintain adequate pressure levels, and pressure variations up to 10 m were observed. Similar conclusions were drawn in Page and Creaco (2019), who reported instability at $\Delta t \leq 1$ min and found optimal behavior of their system at $\Delta t = 3$ min. Galuppini et al. (2019) used a sampling time of 1 s but then concluded that longer sampling intervals might be preferable. In contrast to the these reported findings, other researchers, using transient models, e.g., Prescott and Ulanicki (2003, 2008), AbdelMeguid et al. (2011), Madoński et al. (2014), and Janus and Ulanicki (2018), or based on experimental studies (AbdelMeguid et al. 2011; Fontana et al. 2018), quoted much smaller sampling periods in the range of milliseconds.

The goal of this paper is to highlight the importance of proper selection of sampling times in feedback control systems in general, and specifically when applied to pressure control in WDNs, and to describe the mechanisms by which sampling time can be properly selected and the impact of sampling on stability properly assessed. Initially, basic definitions of stability are given and the reader is introduced to the concept of local stability analysis at equilibrium points via model linearization. Conditions for the stability of linear time-invariant (LTI) systems are given in continuous time as well as discrete time. After the necessary theory is introduced, it is demonstrated how a simple first-order LTI system that is inherently stable becomes unstable following the addition of a feedback loop in which the error signal is sampled with too large a sampling period. It is also shown that it is possible to have a stable closed-loop system with very long sampling periods, provided that the static gain is sufficiently low. However, such a system would also become slower and be less able to follow reference signals and reject disturbances. Subsequently, the results of this simple simulation study become more evident when more theory is introduced and the readers are familiarized with Bode plots and the concepts of bandwidth and stability margins. The main part of this paper is focused on the dynamics of a model of a closed-loop pressure control system with an electronically controlled PRV installed in a full-size WDN described with a transient hydraulic model and solved with a method of characteristics. To design an electronic controller and check its closed-loop stability at different sampling times, the transient model was identified for a number of operating points, producing a family of LTI models represented by transfer functions. As shown, the identified LTI models make it possible to formally describe WDN dynamics. Operation of the designed controllers at different sampling periods was then tested on the transient simulation model using step inputs in the reference signal as well as under time-varying demands.

The work presented here was motivated by a real-life incident that happened in a pressure control scheme in a major UK city and was the subject of a paper by Janus and Ulanicki (2017). Pressure at the inlet of the WDN was controlled by a valve whose position was adjusted by an electromechanical actuator combined in a feedback loop with a proportional integral (PI) controller. It was observed that the gain in the feedback loop increased significantly under small valve openings, causing instability in the system under low-flow conditions. At the same time, it was also observed that stability was sensitive to sampling time.

Nominal and robust stability of pressure control systems was recently discussed in detail in a study by Galuppini et al. (2020), which focused on continuous-time systems, although the effects of sampling were also explained. In contrast, this work deals specifically with discrete-time systems. The analysis was carried out on

reduced models of first order plus delay, although the authors later stressed the need for higher-order models. This work considers a higher-order model with an additional reduction in static nonlinearity via gain compensation. Galuppini et al. (2020) considered a control structure in which the valve position is directly controlled on a pressure reading from a sensor located farther in the network and used a Smith predictor for delay compensation. In practice, it is known that Smith compensators are very sensitive to time delay errors, to the point where, for given robustness levels, standard proportional integral derivative (PID) controllers usually outperform Smith predictors even for simple first-order processes with delay (Sigurd Skogestad 2018). In WDNs, time delays can vary as a result of changes to network topology, e.g., states of isolation valves in the network and the addition/removal of pipes, gradual changes to pipe properties, and possibly also as a result of variability in the distribution of demands across the network. In Galuppini et al. (2020) the reported performance from the Smith predictor was satisfactory.

This work advocates controlling valves based on the pressure signal measurements taken near the valves because of the destabilizing effects of delay, as described in this paper. Since perfect delay compensation is difficult to achieve, positioning pressure sensors away from controlled elements introduces unwanted delay uncertainty and, thus, reduces robustness. Ultimately, the controller needs to have a smaller closed-loop bandwidth to ensure robust stability compared with the scenario where the sensor was positioned closer to the valve. Instead, one could use a cascaded control structure in which a valve is controlled based on a pressure reading taken close to the valve while the setpoint is controlled based on a pressure reading deeper in the network. This configuration allows for the separation of controller dynamics, such that the inner loop controller can be made faster for disturbance rejection (regulation), while a reference tracking (servo) loop can be designed to track slowly varying pressures for leakage management, ultimately resulting in a faster and more robust control system.

Control System Structure

The closed-loop pressure control system used in this study is best described by the block diagram shown in Fig. 1, where arrows represent signals and blocks represent dynamic elements. By convention, signals are functions in time domain t while system dynamics are represented in the complex frequency domains s and z as transfer functions. A brief introduction to transfer functions and Laplace and $\mathcal{Z}$ transforms are provided subsequently in the text. Fig. 1 shows two alternative open-loop paths formed by (a) analog controller $C(s)$, actuator $A(s)$, and plant $P(s)$ and (b) P(s), $C(s)$, and $A(s)$ preceded by a sampler followed by a zero-order hold (ZOH) element with transfer function $G_h(s)$. The measured pressure head $h_d(t)$ downstream of the PRV is fed back to the summation node and compared with the desired reference downstream pressure head $h_{\text{ref}}(t)$. The resulting error signal $e(t) = h_{\text{ref}}(t) - h_d(t)$ forms the input to the controller, which produces the output $u(t)$ driving the actuator that sets the valve position $x_m(t)$. In the case of (b), the error signal is sampled at discrete-time intervals with a sampling period T producing a series of pulses $e(kT)$, where k is an integer. The ZOH block holds the signal constant between each pulse resulting in a stair-shaped error signal $\bar{e}(t)$. During sampling and subsequent ZOH reconstruction, some of the information about the error signal $e(t)$ is irrevocably lost. Instead of the true error value, the controller receives the information outdated by up to one sample. The actuator then sets the valve position $\bar{x}_m(t)$ based on the outdated (between the samples) control signal $\bar{u}(t)$. If the sampling time T is small enough, the difference between the true and the sampled error signal is negligible and the dynamics of the continuous-time and the discrete-time systems are similar. As T becomes larger and the controller acts on more outdated information, the quality of control in the sampled system deteriorates. It is easy to guess that the system is more likely to become unstable if (a) the controller receives more outdated information about the output, i.e., T grows larger, and (b) the controller reacts more strongly upon each computation of the control signal, i.e., the controller is faster.

Stability of Dynamical Systems

If a dynamic system is stable, then the system outputs are bounded within admissible limits under bounded inputs, the so-called bounded input bounded output (BIBO) stability. The converse of the preceding statement, however, may not always be true for reasons that are beyond the scope of this paper (related to the presence of so-called transmission zeros). In water systems, instability of a

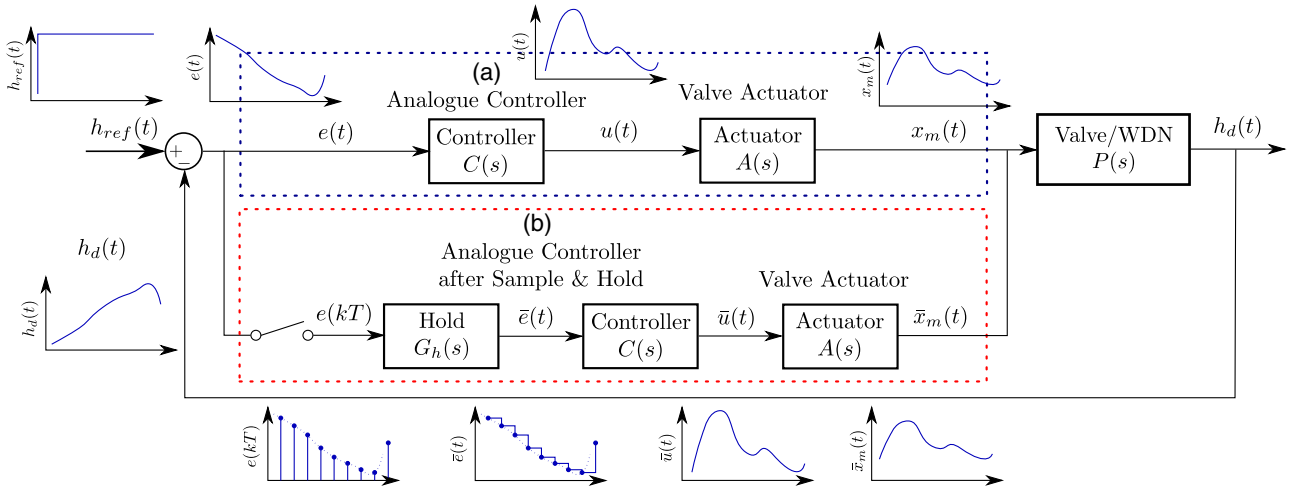

Fig. 1. Control block diagram of closed-loop pressure control scheme in WDN using actuated PRV coupled with analog electronic controller receiving: (a) continuous error signal $e(t)$; and (b) error signal after a sample and hold block $\bar{e}(t)$.

feedback loop may manifest itself through the valve remaining fully open or fully closed (saturation) or through sustained periodic oscillations. Sometimes, a more strict description would be that the system states tend to an equilibrium point of interest (the so-called asymptotic stability). The asymptotic stability of a system implies the previously mentioned BIBO stability. The theory of stability features different problem-specific definitions of stability. This discussion of a feedback control system uses the notion of the stability of a system with respect to its equilibrium points. The discussion is restricted to continuous-time and discrete-time single-input single-output (SISO) systems since a valve/WDN can be regarded as a SISO system, with the valve position x_m being the input and the downstream head at the valve outlet h_d being the output. In continuous time, a SISO control system can be described by the following state-space equations:

$$\dot{\mathbf{x}}(t) = \mathbf{f}(\mathbf{x}(t), u(t)) \tag{1a}$$

$$y(t) = \mathbf{g}(\mathbf{x}(t), u(t)) \tag{1b}$$

where $\mathbf{x}(t) \in \mathbf{R}^n$ is the state vector of the system; $y(t) \in \mathbf{R}$ is the (scalar) output of the system; $u(t) \in \mathbf{R}$ is the (scalar) control input; $\mathbf{f}$ is a continuously differentiable nonlinear function; and $\mathbf{g}$ is a continuous or smooth nonlinear function. In discrete time, a nonlinear SISO control system is described by a discrete-time state-space model of the form

$$\mathbf{x}_{k+1} = \mathbf{f}(\mathbf{x}_k, u_k) \tag{2a}$$

$$y_k = \mathbf{g}(\mathbf{x}_k, u_k) \tag{2b}$$

where all notations are similarly defined; and $k = 0, 1, \ldots$ denote the sample numbers.

An equilibrium point of a system with control input u is a solution to the algebraic set of equations $\mathbf{f}(\mathbf{x}^*, u^*) = 0$ in the case of continuous-time systems and $\mathbf{x}^* = \mathbf{f}(\mathbf{x}^*, u^*)$ in the case of discrete-time systems and is given as a pair $(\mathbf{x}^*, u^*)$. In other words, an equilibrium point is a state of a system in which the derivatives are zero. By definition, $\dot{\mathbf{x}}^* = 0$ and $\dot{u}^* = 0$. In many cases, the foregoing sets of equations are undetermined because different constant control inputs u^* (scalar in case of a SISO system considered here) produces different equilibria $\mathbf{x}^*$ in state space. For the purpose of introducing stability definitions, which are usually given in the literature for systems without control inputs, u^* is removed from $(\mathbf{x}^*, u^*)$ and $\mathbf{x}^*$ referred to as the system's equilibrium point corresponding to some constant given input u^*. Additionally, let the origin of the coordinate system in the state space be shifted such that the nonzero equilibrium point is located at the origin, and let $\mathbf{x}^* = 0$ be treated as the system's equilibrium point corresponding to a constant input u^*.

Then the following definitions of a local stability in the vicinity of an equilibrium point can be formulated. For the continuous-time system described by Eq. (1):

Definition 3.1. **(Stability in continuous time)** *The system* $\dot{\mathbf{x}}(t) = \mathbf{f}(\mathbf{x}(t), u(t))$ *is stable in the sense of Lyapunov about its equilibrium* $\mathbf{x}^* = 0$ *under constant input* u^* *if for any* $\varepsilon > 0$ *and any initial time* t_0 *there exists a ball* $\delta(\varepsilon, t_0) > 0$, *such that* $\|\mathbf{x}(t_0)\| < \delta \Rightarrow \|\mathbf{x}(t)\| < \varepsilon$ *for all* $t \geq t_0$.

Definition 3.2. **(Asymptotic stability in continuous time)** *The system* $\dot{\mathbf{x}}(t) = \mathbf{f}(\mathbf{x}(t), u(t))$ *is asymptotically stable about its equilibrium* $\mathbf{x}^* = 0$ *under constant input* u^* *if it is stable in the sense of Lyapunov and, furthermore, there exists a constant* $\delta = \delta(t_0) > 0$, *such that* $\|\mathbf{x}(t_0)\| < \delta \Rightarrow \|\mathbf{x}(t)\| \to 0$ *as* $t \to \infty$.

Analogously, for the discrete-time system in Eq. (2):

Definition 3.3. **(Stability in discrete-time)** *The system* $\mathbf{x}_{k+1} = \mathbf{f}(\mathbf{x}_k, u_k)$ *is stable in the sense of Lyapunov about its equilibrium* $\mathbf{x}^* = 0$ *under a constant input* u^* *if for any* $\varepsilon > 0$ *and any initial* k_0 *there exists a ball* $\delta(\varepsilon, k_0) > 0$, *such that* $\|\mathbf{x}_{k_0}\| < \delta \Rightarrow \|\mathbf{x}_k\| < \varepsilon$ *for all* $k \geq k_0$.

Definition 3.4. **(Asymptotic stability in discrete-time)** *The system* $\mathbf{x}_{k+1} = \mathbf{f}(\mathbf{x}_k, u_k)$ *is asymptotically stable about its equilibrium* $\mathbf{x}^* = 0$ *under a constant input* u^* *if it is stable in the sense of Lyapunov and, furthermore, there exists a constant* $\delta = \delta(k_0) > 0$, *such that* $\|\mathbf{x}_{k_0}\| < \delta \Rightarrow \|\mathbf{x}_k\| \to 0$ *as* $k \to \infty$ where t_0 is the initial time, k_0 is the initial index, and $\|\cdot\|$ denotes the Euclidean norm. Stability in the sense of Lyapunov means, in simple terms, that a solution that starts near an equilibrium point $\mathbf{x}^*$ will stay near $\mathbf{x}^*$ forever. Asymptotic stability additionally implies that the solution not only stays near $\mathbf{x}^*$ but also converges to it.

Let us now consider the systems in Eqs. (1) and (2), respectively, linearized around the equilibrium point $(\mathbf{x}^*, u^*)$:

$$\dot{\bar{\mathbf{x}}}(t) = \mathbf{A}\bar{\mathbf{x}}(t) + \mathbf{B}\bar{u}(t) \tag{3a}$$

$$\bar{y}(t) = \mathbf{C}\bar{\mathbf{x}}(t) + \mathbf{D}\bar{u}(t) \tag{3b}$$

$$\bar{\mathbf{x}}_{k+1} = \mathbf{A}\bar{\mathbf{x}}_k + \mathbf{B}\bar{u}_k \tag{4a}$$

$$\bar{y}_k = \mathbf{C}\bar{\mathbf{x}}_k + \mathbf{D}\bar{u}_k \tag{4b}$$

where the system matrix $\mathbf{A} = [\partial \mathbf{f}/\partial \mathbf{x}]_{(\mathbf{x}^*, \mathbf{u}^*)}$, the input matrix $\mathbf{B} = [\partial \mathbf{f}/\partial \mathbf{u}]_{(\mathbf{x}^*, \mathbf{u}^*)}$, the output matrix $\mathbf{C} = [\partial \mathbf{g}/\partial \mathbf{x}]_{(\mathbf{x}^*, \mathbf{u}^*)}$, and the feedthrough matrix $\mathbf{D} = [\partial \mathbf{g}/\partial \mathbf{u}]_{(\mathbf{x}^*, \mathbf{u}^*)}$, and $\bar{\mathbf{x}}(t) = \mathbf{x}(t) - \mathbf{x}^*$, $\bar{u}(t) = u(t) - u^*$, $\bar{y}(t) = y(t) - y^*$, $\bar{\mathbf{x}}_k = \mathbf{x}_k - \mathbf{x}^*$, $\bar{u}_k = u_k - u^*$, $\bar{y}_k = y_k - y^*$ are the deviations of the state, input, and output in continuous time and discrete time, respectively.

According to the first Lyapunov criterion, stability analysis of an equilibrium point $(\mathbf{x}^*, u^*)$ can be carried out by studying the stability of the corresponding linearized system in the vicinity of $(\mathbf{x}^*, u^*)$. The criterion applies to continuous-time as well as discrete-time systems.

Theorem 3.1. **(First Method of Lyapunov)** *Consider the two nonlinear dynamic systems in state-space forms defined in* Eq. (1) *(continuous-time) and* Eq. (2) *(discrete-time) and their linearized forms in* Eqs. (3) and (4), *respectively, determined around the equilibrium point* $(\mathbf{x}^*, u^*)$. *For the two considered systems, the following statements hold: If all the eigenvalues of* $\mathbf{A}$ *have negative real parts (in continuous time)/modulus less than one (in discrete time), then the corresponding nonlinear system is asymptotically stable about* $(\mathbf{x}^*, u^*)$. *On the other hand, if* $\mathbf{A}$ *has at least one eigenvalue with a positive real part (in continuous time)/with a modulus greater than one (in discrete time), then the corresponding nonlinear system is unstable around* $(\mathbf{x}^*, u^*)$.

In other words, it is enough to check if a linearized version of a nonlinear system around an equilibrium point is asymptotically stable in order to ensure (local) convergence to that equilibrium point. On the other hand, if the linearized system is unstable, then the original nonlinear system will also be unstable around that equilibrium point. Theorem 3.1 is inconclusive when $\mathbf{A}$ has eigenvalues on the imaginary axis (in continuous time) or with modulus equal one (in discrete time), i.e., for border-line situations; see Strogatz (2007). In these cases, higher-order terms neglected during linearization around the equilibrium point determine whether this equilibrium point is stable or unstable.

One can think of the preceding theorems in the context of a simple pendulum. In a vertically inverted upside-down position with

the center of mass above its pivot point at an angle of 180°, the pendulum is in an unstable equilibrium because the slightest perturbation that causes the angle to deviate from 180° causes the pendulum to fall over and eventually reach a (new) stable equilibrium with the center of mass below its pivot point at an angle 0°, i.e., with the pendulum facing down. The equilibrium is asymptotically stable because it is reached in finite time; see Definitions 3.2 and 3.4. One may imagine a scenario in which the pendulum is in an idealized environment with no air resistance and no friction in the pivot point. If the starting point is with the pendulum in its stable equilibrium, i.e., with the pendulum facing down, and its position deviates by some angle $\varphi| < 180°$, then the pendulum remains oscillating around the stable equilibrium within the bounds $[-|\phi|, +|\phi|]$. The equilibrium is stable because the deviation does not grow in time but is no longer asymptotically stable because it is not be reached in finite time; see Definitions 3.1 and 3.3.

LTI Systems and Frequency Domain

Linear (or linearized) time-invariant systems can be conveniently transformed (under certain conditions, which are beyond the scope of this paper) from time domain t to complex frequency domain $s = \sigma + j\omega$ and from discrete-time domain kT to complex frequency domain $z \overset{\text{def}}{=} e^{sT} = e^{(\sigma+j\omega)T}$. The transformations $y(t) \overset{\mathcal{L}}{\mapsto} Y(s)$ and $y[k] \overset{\mathcal{Z}}{\mapsto} Y(z)$ are carried out using $\mathcal{L}$ and $\mathcal{Z}$ transforms, respectively (Ogata 2010). State-space systems in Eqs. (3) and (4) in the time domain become $Y(s)/U(s) = \mathbf{C}(s\mathbf{I} - \mathbf{A})^{-1}\mathbf{B} + \mathbf{D}$ and $Y(z)/U(z) = \mathbf{C}(z\mathbf{I} - \mathbf{A})^{-1}\mathbf{B} + \mathbf{D}$ in the frequency domain, respectively. The produced algebraic output-input ratios $Y(s)/U(s) = \sum_{k=0}^{M} b_k s^k / \sum_{k=0}^{N} a_k s^k$ and $Y(z)/U(z) = \sum_{k=0}^{M} b_k z^k / \sum_{k=0}^{N} a_k z^k$ are ratios of polynomials in s and z and are called transfer functions $G(s)$ and $H(z)$, respectively. The denominators $D(s) = \sum_{k=0}^{N} a_k s^k$ and $D(z) = \sum_{k=0}^{N} a_k z^k$ of $G(s)$ and $H(z)$ describe the homogeneous parts of their corresponding ordinary differential equation (ODE) and difference equation (DE) and determine their stability. It can be shown, e.g., Ogata (2010), that the roots of $D(s)$ and $D(z)$, henceforth called the poles p_i of $G(s)$ and $H(z)$, are equal to the eigenvalues λ_i of $\mathbf{A}$ when the system has no transmission zeros, i.e., when the state space system is a minimal representation of the transfer function. This is the case for the system studied here, and for this reason, henceforth stability is considered in the frequency domain. Thus, stability conditions for transfer functions are analogous to those for LTI state-space systems; see the First Method of Lyapunov in Theorem 3.1. In continuous time, the transfer function model is stable iff all its poles p_i satisfy the condition $\Re(p_i) = \sigma_i < 0$. In discrete time, the transfer function is stable if all its poles p_i satisfy the condition $|p_i| < 1$. In both cases, the stability is asymptotic.

While pole locations provide information about the absolute stability or lack thereof of a linear or linearized system, relative stability provides information about the proximity of a system to instability after closing the feedback loop and can be calculated or measured in frequency s or z domains. Two stability margins are defined. The gain margin (GM) is the amount of gain that can be added in an open-loop system before a closed-loop system (with added feedback) becomes unstable. The phase margin (PM) is the amount of extra phase lag (phase shift) that is allowed in an open-loop system before a closed-loop system becomes unstable. Both margins can be determined and visualized on Nyquist or Bode plots, and formal GM and PM definitions can be found in, e.g., Ogata (2010). In this paper, Bode plots are used that show the system's gain versus frequency and the system's phase versus frequency on two separate subplots.

The destabilizing effects of gain on pressure control systems was already discussed in Janus and Ulanicki (2018). This paper discusses the destabilizing effects of phase lag, which can be introduced in a system as delays or via sampling. For this purpose, a closed-loop pressure control system is designed for a theoretical WDN. The controller design procedure is as follows. First, the nonlinear valve/WDN system is linearized around the desired equilibrium. Next, linear controllers are designed for the derived linear model at different sampling times. In accordance with Definition 3.1, if the linear model is closed-loop stable, then the nonlinear system in the neighborhood of the equilibrium will be too. Ultimately, the designed closed-loop control systems are checked in a simulation to determine whether the controllers meet the design criteria on the nonlinear model. To prevent the integral of the error from increasing in case the input to the plant saturates due to, for example, nonlinearities such as rate limiters, the controller with integral action needs to be equipped with integrator antiwindup logic.

Stability Analysis of a Simple First-Order Sampled System

Let us visualize how feedback in closed-loop feedback control systems may destabilize an otherwise stable open-loop system when the sampling period is too long or the static gain is too large. For this purpose, the simplest dynamic system is used, i.e., first-order inertia described by a differential equation $\tau dy(t)/dt + y(t) = Ku(t)$ whose transfer function is $G(s) = Y(s)/U(s) = K/(\tau s + 1)$, where K is the static gain and τ the time constant. The closed-loop system shown in Fig. 2 can be viewed as analogous to a feedback pressure control scheme where $G(s)$ represents the inertial response of a rigid-column hydraulic model (Janus and Ulanicki 2017). The system is preceded by a ZOH block with a transfer function $G_h(s) = (1 - e^{-Ts})/s$ and an ideal sampler with sampling period T. The open-loop transfer function

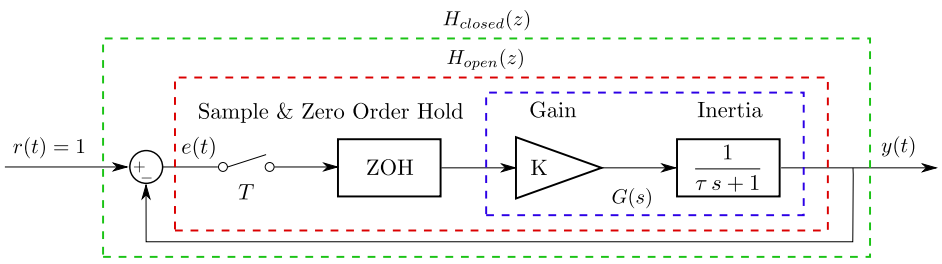

Fig. 2. Feedback control system with first-order dynamics with time constant $\tau = 0.4$ s, and open-loop static gain $K = 2$ and a sample and ZOH block with sampling period T.

J. Water Resour. Plann. Manage., 2021, 147(3): 04021003

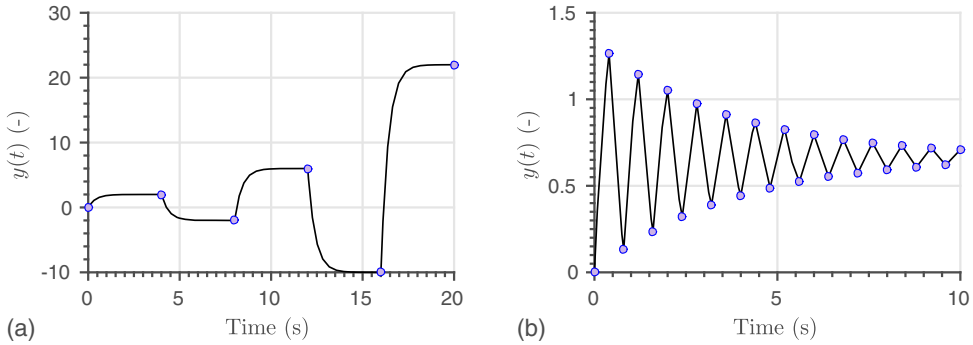

Fig. 3. Time response y of a closed-loop system given in Fig. 2 to a unit step input in r at two different sampling periods T: (a) time response at a sampling period $T = 4$ s; and (b) time response at a sampling period $T = 0.4$ s.

(without feedback) after the sampler can be written $G_{\text{open}}(s) = G_h(s)G(s) = K(1 - e^{-Ts})/[s(\tau s + 1)]$. The open-loop transfer function of the sampled system (including the sampler) can be calculated by taking an inverse $\mathcal{L}$ transform of $G_{\text{open}}(s)$ and then converting the resulting difference equation into the corresponding $\mathcal{Z}$ transfer function, $H_{\text{open}}(z) = \mathcal{Z}\{\mathcal{L}^{-1}[G_{\text{open}}(s)]_{t=kT}\}$. After carrying out the appropriate calculations (e.g., Vande Vegte 1986), the following closed-loop transfer function of the sampled system is obtained:

$$H_{\text{closed}}(z) = K(1 - e^{-T/\tau})/[z - e^{-T/\tau} + K(1 - e^{-T/\tau})] \qquad (5)$$

Since the system is first order, it has a single pole p and is stable if $|p| < 1$. After equating the denominator $D(z)$ to zero, $|p| = |e^{-T/\tau} - K(1 - e^{-T/\tau})| < 1$. Solving the inequality produces the following stability criterion for the sampled first-order system: $T < \tau \ln[(K + 1)/(K - 1)]$. The maximum allowed sampling time depends on the system's time constant τ and the open-loop static gain K. The time constant τ is directly linked to bandwidth in the frequency domain, which is discussed subsequently. The bigger the τ, i.e., the smaller the closed-loop bandwidth, the larger T can get before the system becomes unstable. The relationship versus K is the opposite since K makes the closed-loop response faster, not slower, as in the case of τ. Assume the system has the values $K = 2$ and $\tau = 0.4$ s. The preceding condition gives $T \lesssim T_{\max} = 0.44$ s.

The system's response $y(t)$ to a unit step in the reference signal $r(t) = 1$ was simulated for a sampling period $T = 4$ s sufficiently long to reach new steady-state outputs between samples and for $T = 0.4$ s slightly smaller than the calculated (stable) maximum value. The results plotted in Fig. 3 show that for $T = 4$ s, as expected, the system is unstable and the amplitude of oscillation increases with every sample. In this case, sampling is too infrequent to correct the course of the system, and the absolute value of the error $|e| = |r - y|$ increases with each sample. When T is reduced to a value slightly below $T_{\max}$, the system becomes stable, albeit with frequent oscillations since T is still very close to $T_{\max}$ [Fig. 3(b)]. The response becomes less oscillatory when T is further reduced until it finally resembles an exponential curve. The derived stability criterion can be reordered to find the maximum value of K for a given T: $K < (e^{T/\tau} + 1)/(e^{T/\tau} - 1)$. The system can theoretically be stable for large T provided that K is sufficiently small. This explains how some of the publications quoted in the introduction produced stable solutions at large time steps.

The results in Fig. 3 can be explained without any of the preceding mathematical formalism by looking at the output (y_k) and the error (e_k) values in consecutive samples. The fact that the static gain of $1/(\tau s + 1)$ is equal to one and $T = 4$ s is sufficiently long for the system to attain new steady-state in between the samples is used. Hence, in the kth sample the error $e_k = r_k - x_{k-1}$, while the new steady-state output $y_k = Ke_k$. At the start of the iteration $r_0 = 0$, $e_0 = 0$, and $y_0 = 0$. For $k \geq 1$, $r_k = 1$, representing a unit step in the input. At $K = 2$ and sampling time $T = 4$ s [see Fig. 3(a) and the first time series in Table 1], the steady-state output value at each sample y_k is always twice the current error e_k, which leads to gradual amplification of the error signal and the output itself. The system is unstable. It is intuitive that the system would be stable if the gain $K < 1$, such that the initial error e_k at sample $k = 1$ is gradually attenuated instead of amplified. At $K = 1$ the system is marginally stable and the error and the output signals oscillate between zero and one (see the second time series in Table 1). To turn an unstable closed-loop system into a stable one, the open-loop gain needs to be reduced so that the error signal e_k is attenuated instead of amplified, or, alternatively, one can reduce the sampling time such that the system response does not have time to grow between consecutive control actions. The step response of the system in Fig. 2 at $T = 0.4$ s can be conveniently calculated while taking advantage of the fact that $T = \tau$, where, by definition, time constant τ is the time required for the system to reach $(1 - 1/e) \approx 63.2\%$ of the new steady-state value. Therefore, in the kth sample, $e_k = r_k - y_{k-1}$, while the output at the end of the sample $y_k = y_{k-1} - (y_{k-1} - Ke_k)(1 - 1/e)$. At the end of each sample the output attains only 63.2% of its final value and the error signal $e_k = r_k - x_{k-1}$ becomes smaller than it would have been if the sampling time had been longer. Consequently, the system becomes stable, as shown in Fig. 3(b) and the third time series in Table 1.

Table 1. Output y_k and error e_k values in first 10 iterations of step response of closed-loop system given in Fig. 2 at two different sampling periods T and open-loop static gains K

		$K = 2$, $T = 4$ s		$K = 1$, $T = 4$ s		$K = 2$, $T = \tau = 0.4$ s	
Iteration k	r_k	e_k	y_k	e_k	y_k	e_k	y_k
0	0	0	0	0	0	0	0
1	1	1	2	1	1	1	1.264
2	1	−1	−2	0	0	−0.264	0.131
3	1	3	6	1	1	0.869	1.147
4	1	−5	−10	0	0	−0.147	0.236
5	1	11	22	1	1	0.764	1.052
6	1	−21	−42	0	0	−0.052	0.321
7	1	43	86	1	1	0.679	0.977
8	1	−85	−170	0	0	0.023	0.389
9	1	171	342	1	1	0.611	0.916

Identification of PRV/WDN System

The closed-loop pressure control system was designed for a WDN consisting of a described skeletonized network model with water hammer equations, a static hydraulic model of a PRV, and an inertial model describing the dynamics of the actuator. The combined PRV/WDN model was simulated to generate the input-output data used to identify a family of continuous-time transfer functions between the input to the actuator $u(t)$ and the system output $y(t) = h_d(t)$, i.e., the measured downstream pressure head. Dynamic responses to a unit step in $u(t)$ were computed at different operating points defined by the combination of demands and the downstream pressure $h_d = h_{ref}$ in closed loop. Consequently, a family of transfer functions was identified, covering all tested operating points.

Description of Network Simulation Model

As shown in the schematic diagram in Fig. 4, the network model is composed of 42 pipes and 28 nodes. The pipes between Nodes 4 and 28 are each 75 mm in diameter and 200 m long, while the two pipes upstream and downstream of the PRV are, respectively, 4,000 and 400 m in length and both 200 mm in diameter. It is assumed that pressure waves propagate at a constant celerity $c = 1{,}200$ m/s uniformly across the network. Friction is modeled using a Darcy-Weisbach formula, with the friction factor $f = 2 \times 10^{-4}$ assumed to remain constant within the range of Reynolds numbers observed in the network. The nodes are assigned different elevations ranging between $z_i = 100$ m in Node 3 to $z_i \in [10, 50]$ m in Nodes 4–28.

Demand d_i at each node i is a sum of pressure-independent demand d_i^{pi} and pressure-dependent demand d_i^{pd}. It could be argued that all demands in a transient model should be pressure-dependent since forcing demands independently of pressure does not reflect the physics of fluid flow, which is pressure-driven (Janus and Ulanicki 2017). Doing so leads to overestimation of the magnitude of pressure waves (Jung et al. 2009) and, as shown subsequently in Fig. 5, also the shape of the dynamic response. Though efforts have been made to propose a mathematical description of pressure-dependent demands (Giustolisi and Walski 2012), the application has so far been limited to steady-state WDN analysis. The pressure dependency of demands in non-steady-state conditions is much more elaborate, and since the modeling efforts presented here are aimed only at demonstrating the concept of closed-loop system stability in the practical context of pressure control in WDNs, not at giving an exact description of a particular network, the proposed approach seems adequate. For the same reason, pressure-dependent demand in each node i is calculated using the power equation $d_i^{pd} = C_i(h_i - z_i)^{\alpha}$, where C_i is the pressure-dependent demand coefficient in node i and $\alpha = 1$ is the network-wide pressure-dependent demand exponent, instead of the more accurate fixed and variable area discharges (FAVAD) formula (van Zyl and Cassa 2014). In the unsteady simulation case study, d_i^{pi} was generated using the bottom-up stochastic approach by Buchberger and Wells (1996).

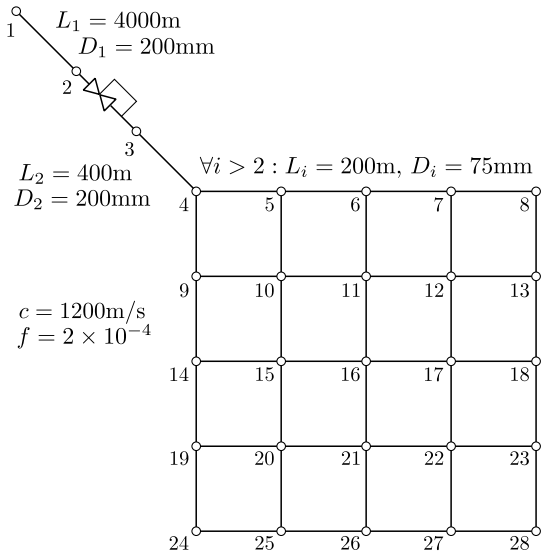

Fig. 4. Schematic diagram of transient WDN simulation model's topology.

Pressure loss in the PRV $\Delta h_{\text{PRV}} = q_m^2/C_v(x_m)^2$, where q_m (m/s^3) denotes the flow across the valve and $C_v(x_m)$ (m m$^{2.5}$/s) is the valve coefficient, which depends on valve opening x_m (%). The valve coefficient $C_v(x_m) = 0.02107 - 0.02962e^{-0.0140x_m} + 0.0109e^{-0.0713x_m} - 0.00325e^{-0.1866x_m} + 0.0009e^{-0.1091x_m}$ is calculated using a regression curve derived from the manufacturer's data. The actuator is described by a first-order transfer function, $A(s) = 1/(\tau_A s + 1)$, where the actuator's time constant τ_A is 0.6 s.

Identification Procedure and Results

Model identification was carried out in MATLAB version 2015b using the System Identification Toolbox function tfest, which, for continuous-time transfer functions estimated on time-domain data, uses state-variable filters (SVFs), combined with the simplified refined instrument variable (IV) method for estimable parameter initialization (Ljung 2009). The transfer function models between the input to the actuator u and the downstream pressure head h_d were identified, one per operating point, for a total number of 18 operating points defined by the pressure-dependent demand coefficient $C_i \in [2, 4, 8] \times 10^{-6}$ m^2/s, pressure-independent demand $d_i^{pi} \in [0.014, 0.026, 0.036]$ m^3/s, and the outlet pressure head setpoint $h_{ref} \in [140,155]$ m. For simplicity, it was assumed that C_i and d_i^{pi} were equal in all nodes at a given operating point. The resulting combinations of d_i^{pi} and C_i produced $q_{pd} \in [0.08q_{\text{tot}}, 0.55q_{\text{tot}}]$, i.e., the pressure-dependent demand constituted between 8% and 55% of the total flow in the network.

After attaining a steady state for a selected combination of C_i, d_i^{pd}, and h_{ref} in closed loop, the feedback loop was removed and a unit step signal $u(t) = 1$ was fed to the actuator in open loop. While the choice of excitation (input) signal for identification is not trivial and there are many options (Ljung 1999), the unit step signal was chosen for its simplicity and ease of interpretation of results in the time domain. The measured output of the transient model, i.e., the pressure head h_d downstream of the PRV, was recorded for each step input. The recorded input-output data were fed to System Identification Toolbox's function tfest to estimate the coefficients a_i and b_i of the continuous transfer function of the form shown by Eq. (6):

$$G(s)A(s) = \frac{b_2 s^2 + b_1 s + b_0}{a_4 s^4 + a_3 s^3 + a_2 s^2 + a_1 s + a_0} \tag{6}$$

$G(s)A(s)$ is a fourth-order transfer function with two zeros and four poles and with one so-called slow pole originating from the actuator dynamics. It could be argued that since the transient hydraulic model used here is infinite-dimensional and has complex wave dynamics, its approximation is likely to be of relatively high order. However, pressure control systems are usually set up with actuators and opening rate limiters having slow enough dynamics

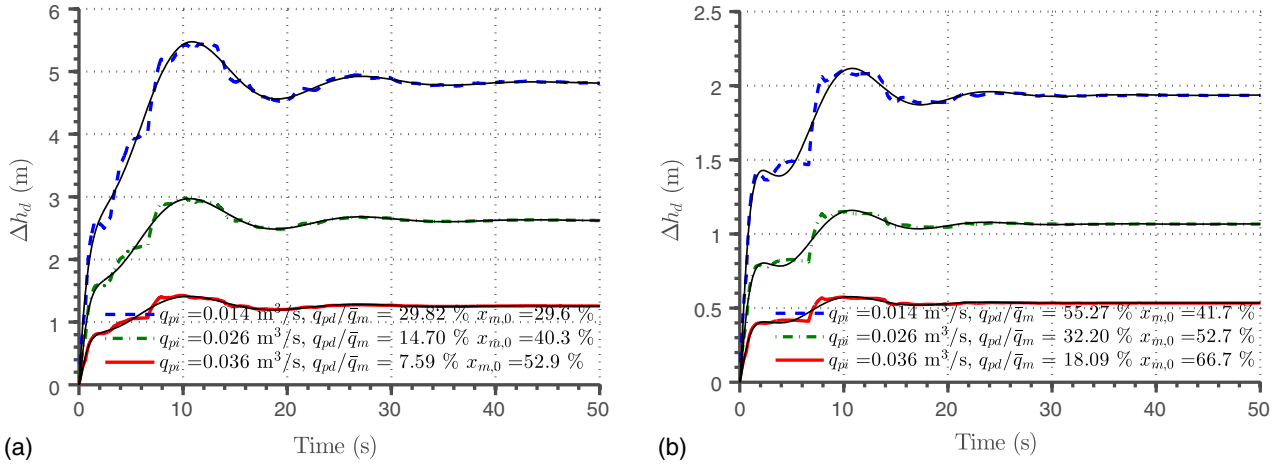

Fig. 5. Outlet pressure responses $\Delta h_d = h_d - h_{d,0}$ from the transient model (bold) and the fitted transfer functions (thin) to a 1% step change in valve position x_m at different pressure-dependent demand coefficients C and pressure independent demands d^{pi}: (a) $C = 2 \times 10^{-6}$ m^2/s; and (b) $C = 8 \times 10^{-6}$ m^2/s.

to prevent induction of faster (higher-order) pressure wave oscillations in the network. These elements act as low-pass filters attenuating higher-order dynamics and producing an overall lower-order dynamic response. It is also hypothesized that higher-order dynamics that can be observed in individual pipes or small networks are less pronounced in larger and more complex networks because the pressure waves are attenuated at individual nodes since the waves meeting each other are likely to have different phases. Since the actuator used in this study has a bandwidth $\omega_A = 1.66$ rad ≈ 0.26 Hz with a 20-dB/decade magnitude roll-off afterwards, any transient frequencies above 1.5 Hz are scaled down to less than 17% of their original amplitudes. The significance of the system having two zeros is that the dynamic response of $G(s)A(s)$ depends not only on the velocity of the valve opening but also on its acceleration.

Fig. 5 shows a plot of 6 out of 18 recorded step responses (bold) with the corresponding outputs from the identified transfer functions (thin). The responses have different static gains, which are dependent on the valve position $x_{m,0}$ at the start of the step experiment, but rather similar dynamics, i.e., rise times, amounts of overshoot, settling times, and peak times. Some difference in dynamic response can be noticed in step responses obtained at higher C values, i.e., with a higher pressure-dependent demand component [Fig. 5(b)]. These responses seem to have a slightly different shape from those obtained for lower C values, plotted in Fig. 5(a), and show distinct steplike departure and arrival moments of the principal pressure wave.

To get a better understanding of the dynamics of the identified transfer functions, their frequency characteristics are plotted in Fig. 6(a) in the form of a Bode plot. The magnitude subplot of the Bode plot shows the differences in amplitudes, i.e., static gains, which largely depend on the valve position, while the phase characteristics are closer together, indicating similar dynamics across the family of the identified models. The only differences in phase characteristics can be observed around approximately 0.5–0.7 rad/s. It is supsected that these frequencies are responsible for the initial part of the time response, and the variability around these frequencies is attributed to the previously mentioned differences in the dynamic response at different C coefficients. For better visualization, the plots were divided into three separate series, plotted with a dashed line for $x_m \leq 35\%$, a solid line for $35\% < x_m \leq 50\%$, and

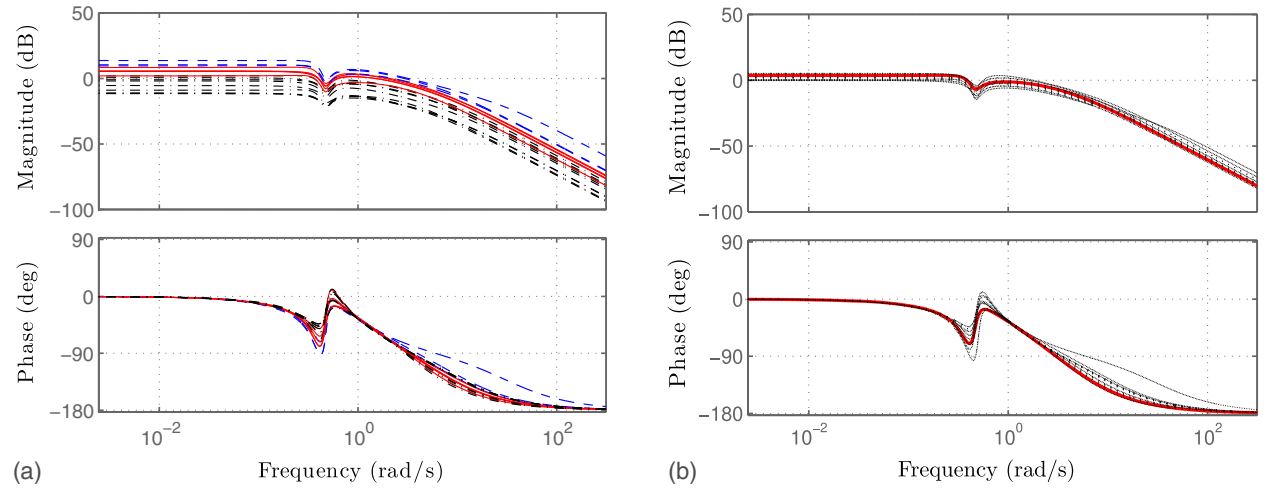

Fig. 6. Frequency characteristics of the family of transfer functions representing the actuator and WDN dynamics at different operating points: (a) original transfer functions; and (b) gain compensated transfer functions.

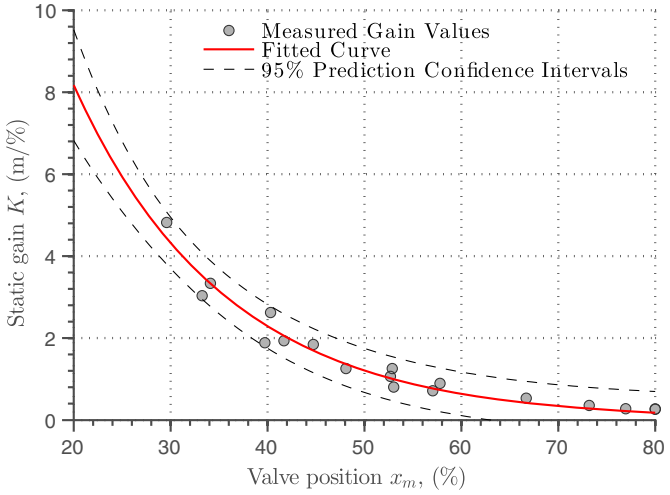

Fig. 7. Dependency of the gain K in the family of identified transfer functions representing the actuator and the WDN system at different operating points on valve position x_m.

a dashed-dotted line for $x_m > 50\%$. The Bode plot was generated up to the Nyquist frequency $\omega_N \approx 157.1$ rad/s $= \pi/0.02$ s where $h = 0.02$ s is the time step in the fixed-step hydraulic solver employed in the method of characteristics. Again, it can be seen that lower gains coincide with higher valve openings while higher gains were recorded under lower valve openings.

Controller Design in Continuous Time

Gain Compensator Design

To keep the open-loop static gain K of the system approximately constant under all operating conditions, the authors implemented the methodology presented in Janus and Ulanicki (2018) and designed a gain compensator block that scales the input to the actuator based on the measurement of the valve position. K values measured during valve operation were plotted against valve position x_m in Fig. 7, together with the fitted regression curve $K(x_m) = p_1 e^{-p_2 x_m}$, where $p_1 = 29.2$ and $p_2 = 0.0636$, with confidence intervals $\langle 19.9, 38.4\rangle$ and $\langle 0.0551, 0.0722\rangle$, respectively. The curve shows a good quality of fit with root-mean-squared error (RMSE) of 0.242, confirming the earlier finding that the static gain of the PRV connected to a WDN is largely dependent on the valve position. Each identified transfer function $G(s)A(s)$ can be described as a product of its static gain K and the dynamic part with unity static gain, as shown by Eq. (7):

$$G(s)A(s) = K\frac{b_2^* s^2 + b_1^* s + 1}{a_4^* s^4 + a_3^* s^3 + a_2^* s^2 + a_1^* s + 1} \tag{7}$$

where $b_i^* = b_i/b_0$ and $a_i^* = a_i/a_0$. Each of the 18 identified transfer functions has a different K, which, when multiplied by the gain compensator $k(x_m)$ defined next, should become close to a typical gain K_{typ} used for controller tuning. As in Janus and Ulanicki (2018), the gain compensator is calculated as follows: $k(x_m) = K(x_m = x_{typ})/K(x_m)$, where x_{typ} denotes a typical (average) valve position (here $x_{typ} = 50\%$), and $K(x_m)$ is the regression curve plotted in Fig. 7. The Bode plot of the gain-compensated system $k(x_m)G(s)A(s)$ is shown in Fig. 6(b). The curves displayed in bold represent the nominal gain-compensated plant and actuator transfer function described by Eq. (8):

$$k(x_m)G(s)A(s) = 1.20\frac{7.944s^2 + 0.8332s + 1.703}{s^4 + 7.036s^3 + 10.06s^2 + 2.971s + 1.355} \tag{8}$$

which was selected from the family of the identified transfer functions for valve position $x_m = 52.9\%$ for which $k(x_m) = 1.20$. Fig. 6(b) demonstrates that the designed gain compensator is effective since the individual magnitude plots now lie much closer together. The steady-state gains of the step responses now fall between 1.0 and 1.8, which means an approximately 6× smaller spread of values compared to the uncompensated system.

Controller Design for Gain-Compensated System

A continuous-time integral (I) controller with transfer function $C(s) = K_i/s$ was tuned using MATLAB's pidtune function on the nominal system given in Eq. (8) for a chosen target 0-dB gain crossover frequency of the tuned open-loop response $\omega_c = 0.15$ rad/s. The crossover frequency ω_c approximately sets the control bandwidth and the closed-loop response time $\approx 1/\omega_c$. The tuned I controller gain $K_i = 0.0985$ leads to a closed-loop system with GM = 36.6 dB at 3.03 rad/s and PM = 74.2° at 0.15 rad/s. In the time domain (not shown), the resulting nominal closed-loop system response has 0% overshoot (OS), zero steady-state error, settling time $t_s = 26$ s, and rise time $t_r = 9.7$ s. The definitions of the preceding terms can be found in one of the control engineering textbooks (e.g., Ogata 2010; Phillips and Harbor 2000; Vande Vegte 1986). The GMs and PMs are significant, which safeguards the system against modeling uncertainties and drift with regard to gain amplification and delay. This indicates a safe and robust controller. The nominal closed-loop transfer function $G_{\text{closed}}(s) = G_{\text{open}}(s)/[1 + G_{\text{open}}(s)]$, where $G_{\text{open}}(s) = 1.20C(s)G(s)A(s)$, is given in Eq. (9) in the zero-pole-gain form, i.e., with factored polynomials in the nominator and the denominator:

$$G_{\text{closed}}(s) = \frac{0.939(s^2 + 0.1049s + 0.2144)}{(s + 5.253)(s + 1.415)(s + 0.1971)(s^2 + 0.1717s + 0.1374)} \tag{9}$$

$G_{\text{closed}}(s)$ is a stable fifth-order system with three real and two complex conjugate poles and two complex conjugate zeros. There are two fast poles, one at −5.3, corresponding to a time constant $\tau = 0.19$ s, and the other at −1.4, i.e., with $\tau = 0.70$ s, and one slow (dominant) real pole at −0.197 ($\tau = 5.1$ s). The two complex conjugate poles producing low-frequency, low-amplitude oscillations are located near the two complex conjugate zeros. These two pairs are responsible for a notch and a peak around 0.37 and 0.46 rad/s, respectively, in the frequency subplot of the Bode plot in Fig. 6(b). The system becomes unstable when the open-loop static gain is magnified 67.6 times, which in log scale is equal to 36.6 dB, i.e., the GM. The nominal closed-loop system has a large stability margin, but nevertheless, as discussed subsequently, becomes unstable when the output/error signal is sampled with $T >$ (15–20) s, i.e., 1.5–2.0 times the closed-loop rise time t_r, which for the nominal system is approximately 9.7 s.

Closed-Loop Performance and Stability in Discrete-Time Domain

Each jth identified open-loop transfer function in continuous time $G_{\text{open},j}(s)$, where $G_{\text{open},j}(s) = k(x_m)K_i/s[G(s)A(s)]_j$, was transformed into an open-loop discrete-time transfer function

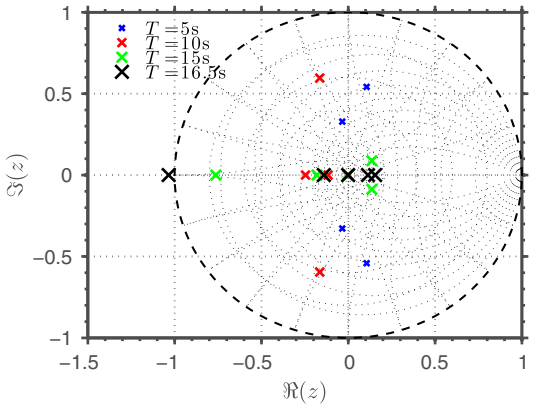

Fig. 8. Pole locations in the $\mathcal{Z}$-plane for the nominal discrete-time closed-loop system $H_{\text{closed}}(z)$ at different sampling periods T.

$H_{\text{open},j}(z)$ at different sampling periods T. The corresponding closed-loop transfer function was then calculated using a formula analogous to the one in continuous time, $H_{\text{closed}}(z) = H_{\text{open}}(z)/[1 + H_{\text{open}}(z)]$. As shown in Fig. 8, the poles of the nominal closed-loop transfer function move away from the origin in the z-plane as T increases until one of the poles goes out of the unit circle for $T \approx 16.5$ s, thus rendering the closed-loop system unstable.

The closed-loop time responses of the family of 18 identified transfer functions with the tuned I controller to a step change in the reference signal h_{ref} are plotted in Fig. 9 for different sampling periods. At $T = 1$ s, the responses have a small, approximately 1% OS and settling times of <40 s. As T increases, the responses become more oscillatory with larger settling times and larger overshoots. At $T = 15$ s the nominal system is still stable, albeit with a large OS of approximately 100% and a settling time exceeding 120 s. Although the nominal system loses stability at $T \gtrsim 16.5$ s (as demonstrated in Fig. 8), some of the systems identified at different operating points are unstable already at $T = 15$ s owing to slight differences in dynamics and imperfect gain compensation.

The performance of the tuned I controller combined with the gain compensator at different sampling was ultimately tested on the transient WDN model. The results in Fig. 10 show that at $T = 1$ s, the closed-loop response is similar to that with the identified transfer function model. It is only slightly more oscillatory owing to some neglected fast dynamics in the transfer function approximation. The similarity begins to fall apart at larger sampling periods for which the transient PRV/WDN becomes unstable already at $T = 10$ s, while at $T = 5$ s it is already quite oscillatory with OS of up to 70%. Dynamics neglected during the identification of (lower-order) transfer functions begin to play a role in the overall discrete-time system stability, however at already long and practically infeasible sampling periods. At $T = 0.25$ s the closed-loop performance with the transient WDN model is very similar to that with the identified transfer function and to the continuous time system. This suggests that, for this particular controller, the system should be sampled with $T \approx 0.25$–0.30 s and not less frequently than $T = 1$–1.5 s, or otherwise stability margins would be significantly reduced in comparison to their designed values and the overall system response would become oscillatory up to the point of eventually becoming unstable.

Reduction of closed-loop stability margins at larger sampling periods and static gains are visualized in Bode plots in Fig. 11 describing the nominal plant in open loop with the tuned I controller. As previously, the plots are generated up to the Nyquist frequency marked with a vertical solid line. The closed-loop system's PM is the additional amount of phase lag that is required for the open-loop system's phase to reach $-180°$ at the gain crossover frequency ω_{gc}, i.e., the frequency where the open-loop system's magnitude is 0 dB.

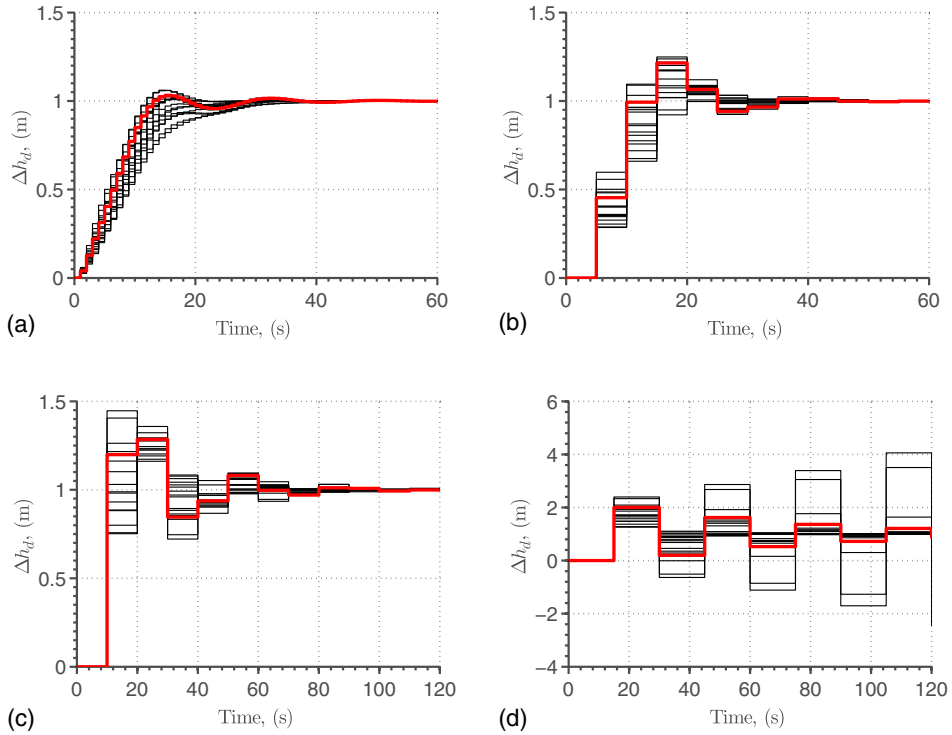

Fig. 9. Closed-loop responses of sampled system with different sampling periods T and at different operating points represented by different identified transfer function models: (a) $T = 1$ s; (b) $T = 5$ s; (c) $T = 10$ s; and (d) $T = 15$ s.

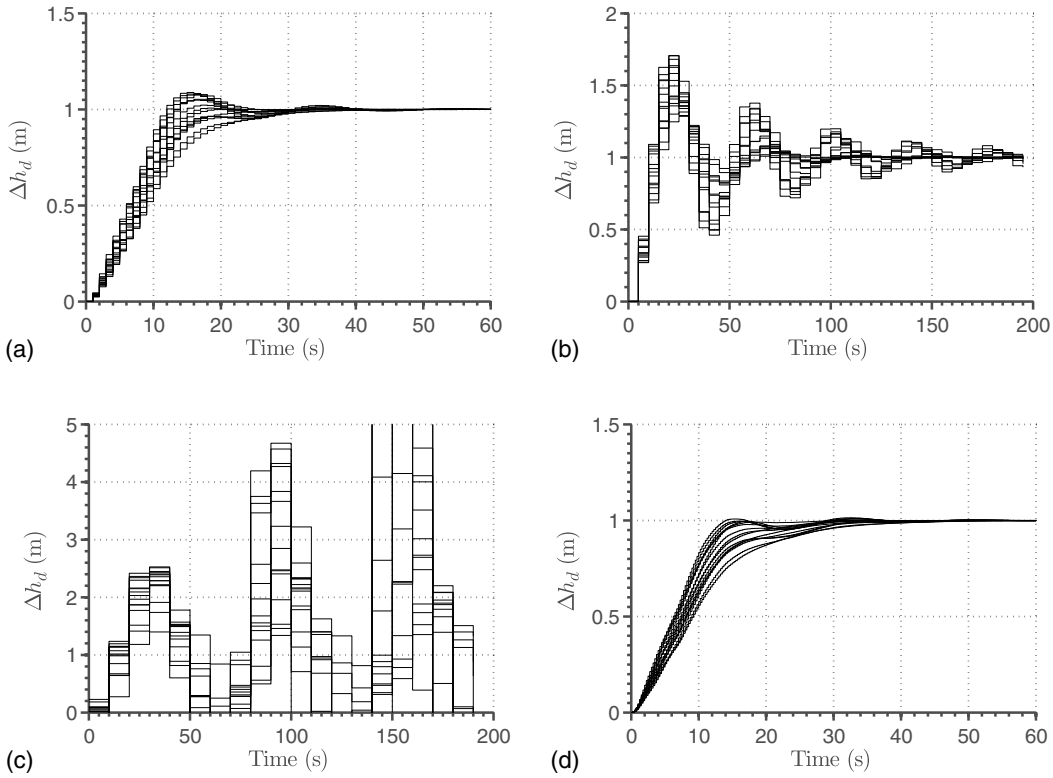

Fig. 10. Closed-loop responses of sampled system with different sampling periods T and at different operating points using transient simulation model: (a) $T = 1$ s; (b) $T = 5$ s; (c) $T = 10$ s; and (d) $T = 0.25$ s.

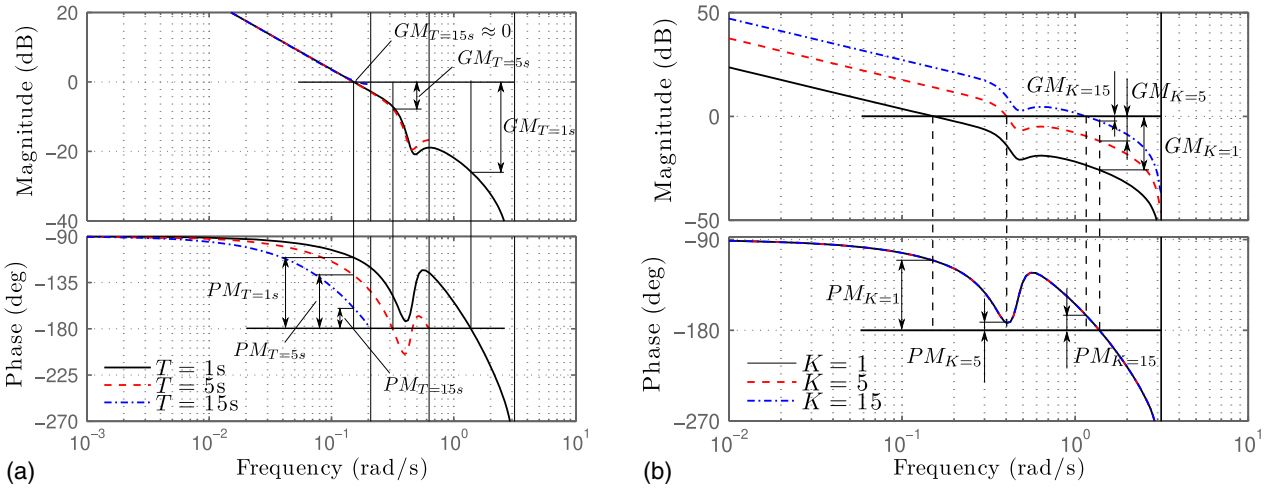

Fig. 11. Bode plots of open-loop system used to generate closed-loop step responses showing dependence of PMs and GMs on sampling time T and static gain K: (a) magnitude and phase characteristics at different sampling times T; and (b) magnitude and phase characteristics at different static gains K.

Likewise, the GM is the additional amount of gain required for the open-loop system's magnitude to reach 0 dB at the phase crossover frequency ω_{pc}, i.e., the frequency where the open-loop system's phase equals $-180°$. As can be seen in Fig. 11, increasing the sampling time curves the phase plot downward while the magnitude plot remains relatively unchanged up to frequencies close to the Nyquist frequency. Consequently, the PM is reduced as the phase curve lies closer to $-180°$ (from above) and the GM is also reduced owing to the fact that phase crossover occurs at lower frequencies ω_{pc}, and for most physical systems the magnitude of a transfer function decreases with frequency. This global trend can be reversed locally since the function may not always be monotonic, as further described subsequently. On the other hand, increasing the static gain shifts the magnitude plot upward while the phase plot remains the same. Consequently, GM decreases as the magnitude plot lies closer to 0 dB (from below), while the PM is usually reduced because it is evaluated at higher gain crossover frequencies ω_{gc} and phase decreases with frequency, albeit not always monotonically, as mentioned previously with regard to the magnitude plot. In this case study, one can see a notch and a peak for frequencies $\omega \approx 0.3$–1.1 rad/s owing to the effects of wave dynamics on top of inertial dynamics. As a result, the

phase locally increases for $\omega \approx 0.5-1.1$ rad/s. Consequently, the PM will not change monotonically with static gain, and one can have a larger PM for $K = 10$ than for $K = 5$. However, it should be borne in mind that this study used a family of models with different frequency characteristics, depending on the operating point [Fig. 6(b)], and with significant differences in phase plots between the models in this particular frequency range. Additionally, the system needs to be safeguarded against the effects of unmodeled dynamics, and thus, for this particular sampling period $T = 1$ s, it would be undesirable to design a controller with a closed-loop bandwidth $\omega_c \approx \omega_{gc} \gtrsim 0.15$ rad/s. As static gain is increased, so is the gain crossover frequency ω_{gc} while the phase crossover frequency ω_{pc} remains the same. Since $\omega_{gc} < \omega_c < \omega_{pc}$, but as a rule of thumb $\omega_c \approx \omega_{gc}$, as static gain is increased, so is the closed-loop bandwidth ω_c, and thus one has a closed-loop system which is more responsive to inputs of higher frequencies.

Case Study

Controller Design at Different Sampling Intervals

As discussed previously, for a given controller with constant parameters, there exists a maximum sampling period beyond which the closed-loop system becomes unstable. In order to be able to use larger sampling periods while keeping the system robust, i.e., stable and with sufficient GMs and PMs, the response of the open-loop system needs to be made slower or, in frequency-domain terminology, the target closed-loop bandwidth ω_c needs to be reduced. To find the target ω_c value for a given discrete controller with sampling time T it is be assumed that ω_c is a fraction f_{ω_c} of the Nyquist frequency π/T, that is

$$\omega_c = \frac{\pi}{f_{\omega_c} T}$$

The GMs and PMs of the systems designed with integral (I) controllers at different T = (1, 5, 15, 60) s and f_{ω_c} are plotted in Fig. 12. As f_{ω_c} increases, so do the PMs and GMs of a discrete-time system. To safeguard against static gain increase, a target GM of approximately 15–25 dB requires $f_{\omega_c} \approx 25$. For this value of f_{ω_c}, the PM is approximately 75°–85°. For a given f_{ω_c}, PMs tend to be smaller for systems designed for higher target

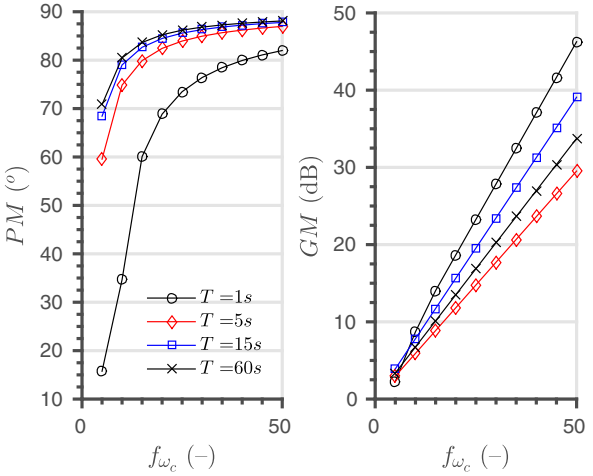

Fig. 12. PMs and GMs for systems designed with different target sampling times T and different target closed-loop bandwidths ω_c defined by a fraction f_{ω_c} of Nyquist frequency π/T.

ω_c owing to the presence of higher-order dynamics in the dynamic response. At lower target ω_c values ($T = 15$ and 60 s), the valve/WDN response is approximately inertial and the PM curves in Fig. 12 are near each other. In this case study, $f_{\omega_c} = 25$ and the resulting target $\omega_c = 1.257 \times 10^{-1}, 2.513 \times 10^{-2}, 8.378 \times 10^{-3}, 2.094 \times 10^{-3}, 6.981 \times 10^{-4}, 4.189 \times 10^{-4}$ rad/s for each target T, respectively. The resulting I controller gains for each T are respectively as follows: $K_i = 8.274 \times 10^{-2}, 1.666 \times 10^{-2}, 5.555 \times 10^{-3}, 1.389 \times 10^{-3}, 4.629 \times 10^{-4}, 2.777 \times 10^{-4}$ m/(%s). As can be seen in Fig. 6(b) the chosen target frequencies are below the frequencies of some key system dynamics present at $\omega > 0.1$ rad/s, which approximate the wave dynamics of the full (transient) system. Thus, it can be expected, and can be verified via simulation, that the designed closed-loop system would not be able to compensate for some transient effects owing to sudden demand changes. Since the target closed-loop system responses are slow, the I controller suffices to satisfy the desired response, and addition of proportional (P) and derivative (D) terms of the PID controller did not lead to any improvements to the overall response of the closed-loop system. To compare the performance of the aforementioned closed-loop systems against those with faster loop dynamics, three controllers at $T = 0.1, 0.20, 0.50$ s were also designed. Larger bandwidths and presence of higher-order dynamics necessitated using higher-order (PID) controllers. The calculated gain triplets (K_p, K_i, K_d) for the three controllers are (1.308, 2.324, 0.1840), (1.018, 0.2724, 0.2083), and (0.1422, 0.1277, 0), respectively. These controllers (in continuous time) were chosen to guarantee infinite GMs and PM = 80° at $\omega_c = 2$, 0.4, and 0.2 rad/s, respectively. It can be seen in Fig. 6(b) that $\omega_c = 2$ rad/s lies to the right of the notch and peak in the phase plot representing some crucial system dynamics, and therefore, it is expected that the system will be better able to reject higher-frequency disturbances. The choice of target ω_c values was less automated than in the former case with longer sampling times and necessitated some manual iterations to satisfy the chosen stability margins and response characteristics in the presence of more complex (wave) dynamics in the system. The resulting step responses exhibit OSs of <2.5% for $T = 0.2$ and 0.5 s and 5% for $T = 0.01$ s. The rise times t_r are 0.91, 5.99, and 8.86 s, which means that the designed discrete-time systems sample 90, 30, and 18 times per rise time, respectively.

The closed-loop step responses to a 1% step in the reference signal h_{ref} for all designed controllers are shown in Fig. 13. The closed-loop control loops show overdamped or slightly underdamped responses with (dominant) time constants growing with T. Performance of the designed pressure control schemes with

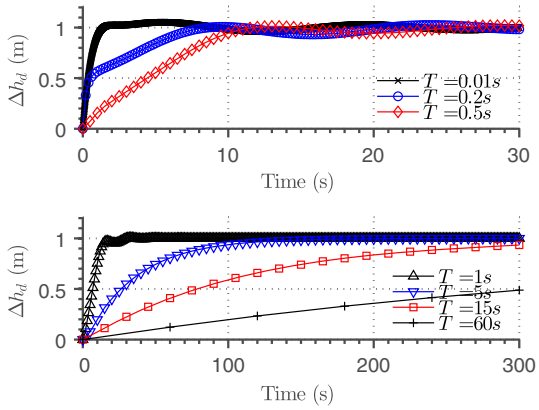

Fig. 13. Closed-loop responses of sampled systems with different controllers and different sampling periods T.

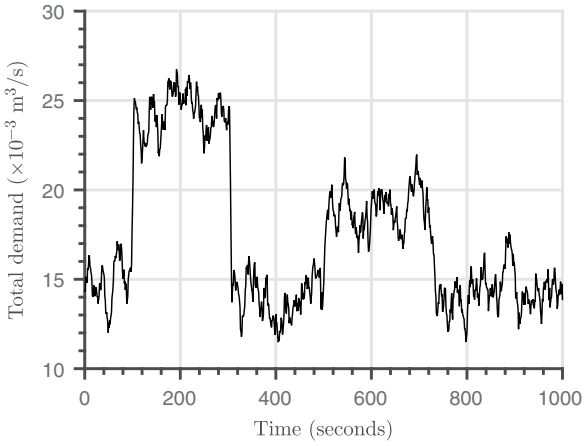

Fig. 14. Total pressure-independent demand profile across WDN used in case study.

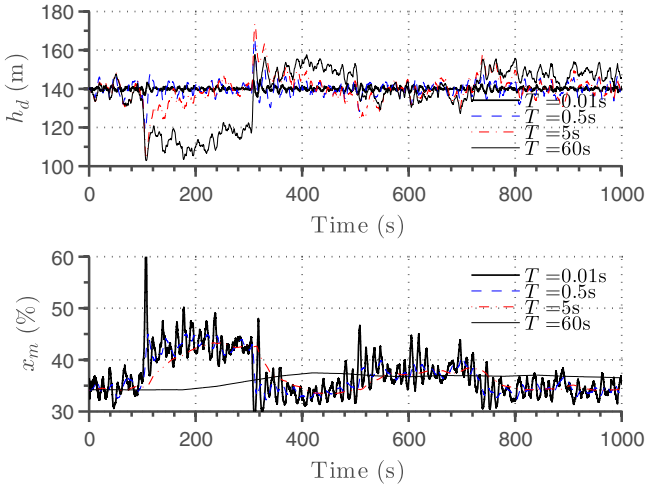

Fig. 15. Downstream head h_d during simulation under time-varying demands in closed-loop pressure control system with different controllers and sampling times.

different bandwidths and sampling intervals was tested under time-varying conditions with a transient simulation model. For this purpose the authors generated separate realistic demand profiles for all nodes of the WDN that take into account random smaller intensity flow fluctuations from residential areas as well as larger sudden demands from an industrial user and those due to hydrant opening.

Demand Profile

The residential demand profile was generated for each demand node of the network using the bottom-up stochastic approach proposed by Buchberger and Wells (1996), where the demand events in a residence are represented by a series of rectangular pulses, each with an arrival time, an intensity, and a duration. As in Buchberger and Wells (1996) the arrival times were represented by a Poisson process. The duration and intensity of each event were assigned random values according to exponential and normal distributions, respectively, as in Prescott and Ulanicki (2008). It was assumed that each of the 25 demand nodes, i.e., Nodes 4–28 in Fig. 4, supplies 120 houses, giving a total of 3,000 houses. A series of Poisson events was generated for each house over the duration time of 1,000 s. Parameter values from Prescott and Ulanicki (2008) were used, i.e., mean interevent time of 5 min, average event duration of 15 s, and average event intensity of 6 L/min. The resulting demand pulse series for each house were then aggregated to yield a residential demand pattern for each node. In addition, two rapid water uptake events were added to the demand profiles in Nodes 13 and 20. In Node 20, a hydrant is opened after 100 s producing a $10-\mathrm{L/s}$ increase in water demand over a 5-s period and remaining at this value for 200 s, after which the hydrant is shut down, again over a 5-s period. A smaller and a more gradual increase in water demand is simulated in Node 13, where a single industrial user is assumed to create a $5-\mathrm{L/s}$ increase in demand over 20 s at the simulation time of 500 s, remaining at this value for an additional 200 s and decreasing to 0 L/s over the next 20 s. The two aforementioned events were added to the residential profiles in Nodes 13 and 20, respectively. The total (aggregated) demand profile is shown in Fig. 14.

Results

The simulated pressure heads h_d downstream of the valve for the selected closed-loop systems with sampling times $T = 0.01, 0.5, 5,$ and 60 s are plotted in Fig. 15. As suspected, the higher the sampling time (and the lower the target closed-loop crossover frequency ω_c to guarantee the desired stability margins), the slower the response time of the system to incoming disturbances, i.e., pressure waves caused by demand changes. At $T = 0.5$ s, the controller is able to maintain $h_d \approx h_{set} = 140$ m throughout the simulation, but temporary variations up to approximately 20 m and lasting for about 20 s are visible as the system is unable to counteract the effects of incoming pressure waves. At $T = 5$ s the sudden variations are slightly higher and up to approximately 30 m, while at the same time the system takes longer to recover and settle to the setpoint. At $T = 60$ s the pressure changes are up to approximately 30–35 m, but the closed-loop bandwidth is small enough that also lower-frequency disturbances are not rejected and periods with inadequate downstream pressure last for up to 200 s. At longer sampling times in the range of minutes, it is expected that the periods with inadequate pressure would become longer, depending on the frequency characteristics of the demand pattern in the network. Ultimately, at $T = 0.01$ s, the controller designed with target $\omega_c = 2$ rad/s is able to better reject higher-frequency disturbances, and consequently, h_d stays closer to the setpoint without longer-term divergences and only occasional ± 4 m variations lasting for seconds. At even larger closed-loop bandwidths, it is expected that the disturbance rejection characteristics of the system will improve further, and thus, the variability of the outlet pressure will be reduced even more. However, the overall performance will depend on the designed controller and its gains and the speed of the actuator, which will need to be set following formal controller design procedures and testing. Variability in the output $y = h_d$ was measured as a mean integral squared error (MISE) defined as

$$e_{y,\mathrm{MISE}} = \frac{1}{t_{\mathrm{simu}}} \int_0^{t_{\mathrm{simu}}} \left(\frac{h_d(t) - h_{ref}}{h_{ref}} \right)^2 dt$$

where t_{simu} = simulation time; and h_{ref} is the reference signal (pressure setpoint). Control effort was measured as mean sum of squares (MSS):

$$Q_{u,\mathrm{MSS}} = \frac{1}{N} \sum_{i=1}^{i=N} \left(\frac{x_m^i - x_{m,0}}{x_{m,0}} \right)^2$$

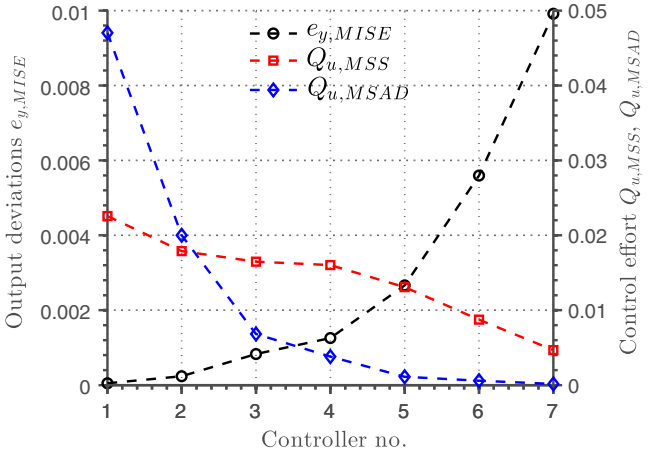

Fig. 16. Errors in output signal $y = h_d$ (measured as mean integral squared error (MISE), and control effort $u = x_m$, measured as mean sum of squares (MSS) and mean sum of absolute derivatives (MSAD) for feedback control systems implemented with different controllers and with different sampling periods T.

and mean sum of absolute derivatives (MSAD):

$$Q_{u,\mathrm{MSAD}} = \frac{1}{t_{\mathrm{simu}}} \sum_{i=2}^{i=N} \left| \frac{x_m^i - x_m^{i-1}}{x_{m,0}} \right|$$

where x_m^i denotes the valve position at the ith time instant; N is the number of discrete-time instants; and $x_{m,0}$ is the (steady-state) valve position at the beginning of the simulation. $Q_{u,\mathrm{MSS}}$ measures the energy spent on actuating the valve, i.e., control costs, while $Q_{u,\mathrm{MSAD}}$ measures the variability of the controller output and can be used to measure the expected intensity of the wear of the mechanical components, i.e., the actuator and the control element; $e_{y,\mathrm{MISE}}$, $Q_{u,\mathrm{MSS}}$, and $Q_{u,\mathrm{MSAD}}$ are plotted in Fig. 16 for all seven controllers with sampling times of 0.01, 0.20, 0.50, 1, 5, 15, and 60 s, respectively. As the feedback control system becomes slower (i.e., has a smaller closed-loop bandwidth), the larger the output errors become because the system is unable to reject disturbances of higher frequencies. On the other hand, faster controllers maintain the setpoint more closely but produce more control action, resulting in higher values of $Q_{u,\mathrm{MSS}}$ and $Q_{u,\mathrm{MSAD}}$. $Q_{u,\mathrm{MSS}}$ is a measure of energy spent on actuation. It can be seen that the increase in $Q_{u,\mathrm{MSS}}$ is substantially smaller than the improvement in the overall system performance. $Q_{u,\mathrm{MSAD}}$, on the other hand, is a measure of the speed of movement of the valve element and determines the power requirements of the actuator. Fig. 16 shows that the plots for $Q_{u,\mathrm{MSAD}}$ and $e_{y,\mathrm{MISE}}$ are of a similar shape but have opposite gradients. Achieving better disturbance rejection requires more powerful actuators and comes at a cost of higher wear due to more action, especially during time periods with large variability in demand. It is intuitive to think that in time periods with less variability in demand the additional amount of control action required by faster controllers compared to slower ones should be proportionally smaller. A faster controller operating at shorter sampling times will act on smaller deviations in the error signal, while controllers operating at longer sampling times will eventually let the error signal build in the system and may require larger error corrections.

Conclusion

As demonstrated in this paper, closed-loop feedback control systems can be destabilized by increasing gain or via delays. Such delays may derive from the properties inherent in the control system, e.g., backlash in mechanical systems, communication delays in control loops, sensors located far from actuators, or, in the case of discrete-time systems, from sampling. In discrete-time control, a practical rule of thumb states that the sampling period $T \leq t_r/10$, where t_r is the closed-loop rise time. An analogous criterion can be formulated in the frequency domain, where the Nyquist frequency $\omega_N = \pi/T$ needs to be larger than $10\omega_c$–$50\omega_c$, ω_c being the desired bandwidth of the closed-loop system. In the case of the I controller designed in the first half of this paper with the target $\omega_c = 0.15$ rad/s, the resulting closed-loop rise time $t_r = 8 - 15$ s. Therefore, the choice of sampling time $T \lesssim 0.8$ s should theoretically produce good performance in the worst-case scenario. Step experiments with the transient model produced good transient response at $T = 1$ s, while the output closely resembled the desired response in continuous time at $T = 0.25$ s. A loss of stability occurred at $T \approx 10$ s, i.e., $T \approx t_r$. $T = 1$ s corresponds to $\omega_N \approx 2.1\omega_c$ based on the ω_c of the nominal system.

The speed of a closed-loop response, measured by response time in the time domain or closed-loop bandwidth ω_c in the frequency domain, can be decreased by reducing the open-loop gain, as demonstrated initially on a closed-loop feedback system with open-loop inertial dynamics. Consequently, long sampling times can be used in feedback systems while still maintaining closed-loop stability provided that the open-loop static gain is sufficiently small, as is the case in the bulk of the published works on the RTC of WDNs (e.g., Creaco et al. 2019). Nevertheless, as the gain decreases, the effects of feedback are reduced and the closed-loop system becomes less effective at rejecting disturbances and following setpoints at lower frequencies up to the point where the system can no longer meet the desired performance criteria.

Simulations with the transient hydraulic WDN model with time-varying demand patterns demonstrated how the speed of the response of a closed-loop system, calculated for stability and robustness for each sampling period, affects the ability of the pressure control system to maintain the desired outlet pressure under transient conditions. In the case $T = 0.01$ s, the closed-loop bandwidth of 2 rad/s is large enough that the system can react to the bulk of the frequencies describing the wave (transient) dynamics, and thus, the impacts of the incoming pressure waves are substantially reduced. Consequently, the outlet pressure is kept near the desired value. As the sampling time is increased, requiring lower closed-loop bandwidths, i.e., controller speeds, the closed-loop system becomes less responsive to disturbances, which manifests as larger downstream pressure variations around the setpoint and longer times with inadequate outlet pressure.

Identification of the transient WDN model coupled with the electrically actuated PRV under study revealed that the relationship between the valve position and the downstream head could be described by a family of fourth-order transfer functions having similar dynamics at all operating points and different static gains that depend largely on valve position. For controller design purposes, this family of transfer functions could be approximated with a single (nominal) transfer function multiplied by the gain versus valve position curve, as suggested in Janus and Ulanicki (2018). The feedback controller could therefore be designed on the nominal transfer function and implemented in the real system in combination with the gain compensator, whose purpose is to adjust the gain of the controller depending on the valve position, such that the overall static gain of the open-loop system is approximately constant at all operating points.

Data Availability Statement

The following data, models, or code generated or used during the study are available from the corresponding author by request:

- simple first-order sampled system in Simulink used to demonstrate the mechanisms of instabilities in feedback systems,
- PRV/WDN system in Simulink used for model identification and final simulation under time-varying demand,
- family of identified transfer functions used for controller design, and
- code for generation of demand patterns as stochastic series of pulses.

References

AbdelMeguid, H., P. Skworcow, and B. Ulanicki. 2011. "Mathematical modelling of a hydraulic controller for PRV flow modulation." *J. Hydroinf.* 13 (3): 374–389. https://doi.org/10.2166/hydro.2011.024.

Berardi, L., A. Simone, D. B. Laucelli, R. M. Ugarelli, and O. Giustolisi. 2018. "Relevance of hydraulic modelling in planning and operating real-time pressure control: Case of Oppegård municipality." *J. Hydroinf.* 20 (3): 535–550. https://doi.org/10.2166/hydro.2017.052.

Buchberger, S. G., and G. J. Wells. 1996. "Intensity, duration, and frequency of residential water demands." *J. Water Resour. Plann. Manage.* 122 (1): 11–19. https://doi.org/10.1061/(ASCE)0733-9496(1996)122:1(11).

Campisano, A., E. Creaco, and C. Modica. 2010. "RTC of valves for leakage reduction in water supply networks." *J. Water Resour. Plann. Manage.* 136 (1): 138–141. https://doi.org/10.1061/(ASCE)0733-9496(2010)136:1(138).

Campisano, A., C. Modica, S. Reitano, R. Ugarelli, and S. Bagherian. 2016. "Field-oriented methodology for real-time pressure control to reduce leakage in water distribution networks." *J. Water Resour. Plann. Manage.* 142 (12): 04016057. https://doi.org/10.1061/(ASCE)WR.1943-5452.0000697.

Campisano, A., C. Modica, and L. Vetrano. 2012. "Calibration of proportional controllers for the RTC of pressures to reduce leakage in water distribution networks." *J. Water Resour. Plann. Manage.* 138 (4): 377–384. https://doi.org/10.1061/(ASCE)WR.1943-5452.0000197.

Creaco, E. 2017. "Exploring numerically the benefits of water discharge prediction for the remote RTC of WDNs." *Water* 9 (12): 961. https://doi.org/10.3390/w9120961.

Creaco, E., A. Campisano, N. Fontana, G. Marini, P. Page, and T. Walski. 2019. "Real time control of water distribution networks: A state-of-the-art review." *Water Res.* 161 (Sep): 517–530. https://doi.org/10.1016/j.watres.2019.06.025.

Creaco, E., A. Campisano, M. Franchini, and C. Modica. 2017. "Unsteady flow modeling of pressure real-time control in water distribution networks." *J. Water Resour. Plann. Manage.* 143 (9): 04017056. https://doi.org/10.1061/(ASCE)WR.1943-5452.0000821.

Creaco, E., A. Campisano, and C. Modica. 2018. "Testing behavior and effects of PRVs and RTC valves during hydrant activation scenarios." *Urban Water J.* 15 (3): 218–226. https://doi.org/10.1080/1573062X.2018.1424214.

Creaco, E., and M. Franchini. 2013. "A new algorithm for real-time pressure control in water distribution networks." *Water Supply* 13 (4): 875–882. https://doi.org/10.2166/ws.2013.074.

Fontana, N., M. Giugni, L. Glielmo, G. Marini, and R. Zollo. 2018. "Real-time control of pressure for leakage reduction in water distribution network: Field experiments." *J. Water Resour. Plann. Manage.* 144 (3): 04017096. https://doi.org/10.1061/(ASCE)WR.1943-5452.0000887.

Galuppini, G., E. Creaco, C. Toffanin, and L. Magni. 2019. "Service pressure regulation in water distribution networks." *Control Eng. Pract.* 86 (May): 70–84. https://doi.org/10.1016/j.conengprac.2019.03.007.

Galuppini, G., L. Magni, and E. Creaco. 2020. "Stability and robustness of real-time pressure control in water distribution systems." *J. Hydraul. Eng.* 146 (4): 04020023. https://doi.org/10.1061/(ASCE)HY.1943-7900.0001722.

Giustolisi, O., R. M. Ugarelli, L. Berardi, D. B. Laucelli, and A. Simone. 2017. "Strategies for the electric regulation of pressure control valves." *J. Hydroinf.* 19 (5): 621–639. https://doi.org/10.2166/hydro.2017.101.

Giustolisi, O., and T. M. Walski. 2012. "Demand components in water distribution network analysis." *J. Water Resour. Plann. Manage.* 138 (4): 356–367. https://doi.org/10.1061/(ASCE)WR.1943-5452.0000187.

Janus, T., and B. Ulanicki. 2017. "Hydraulic modelling for pressure reducing valve controller design addressing disturbance rejection and stability properties." *Procedia Eng.* 186: 635–642. https://doi.org/10.1016/j.proeng.2017.03.280.

Janus, T., and B. Ulanicki. 2018. "Improving stability of electronically controlled pressure-reducing valves through gain compensation." *J. Hydraul. Eng.* 144 (8): 04018053. https://doi.org/10.1061/(ASCE)HY.1943-7900.0001498.

Jones, S., R. Collins, and J. Boxall. 2015. "Do transients contribute to turbidity failures of water distribution systems?" In *Proc., BHR Group—12th Int. Conf. on Pressure Surges*. Dublin, Ireland: BHR Group. https://doi.org/10.13140/RG.2.1.4667.9122.

Jung, B. B. S., P. F. Boulos, and D. J. Wood. 2009. "Effect of pressure-sensitive demand on surge analysis." *Am. Water Works Assoc. J.* 101 (4): 100–111. https://doi.org/10.1002/j.1551-8833.2009.tb09877.x.

Ljung, L., ed. 1999. *System identification: Theory for the user.* 2nd ed. Upper Saddle River, NJ: Prentice Hall.

Ljung, L. 2009. "Experiments with identification of continuous time models." *IFAC Proc. Vol.* 42 (10): 1175–1180. https://doi.org/10.3182/20090706-3-FR-2004.00195.

Madoński, R., M. Nowicki, and P. Herman. 2014. "Application of active disturbance rejection controller to water supply system." In *Proc., 33rd Chinese Control Conf.*, 4401–4405. New York: IEEE. https://doi.org/10.1109/ChiCC.2014.6895677.

Malppan, P. J., and K. Sumam. 2015. "Pipe burst risk assessment using transient analysis in surge 2000." *Aquatic Procedia* 4: 747–754. https://doi.org/10.1016/j.aqpro.2015.02.157.

Ogata, K. 2010. *Modern control engineering*. 5th ed. Harlow, UK: Pearson.

Page, P. R., A. M. Abu-Mahfouz, and M. L. Mothetha. 2017a. "Pressure management of water distribution systems via the remote real-time control of variable speed pumps." *J. Water Resour. Plann. Manage.* 143 (8): 04017045. https://doi.org/10.1061/(ASCE)WR.1943-5452.0000807.

Page, P. R., A. M. Abu-Mahfouz, and S. Yoyo. 2017b. "Parameterless remote real-time control for the adjustment of pressure in water distribution systems." *J. Water Resour. Plann. Manage.* 143 (9): 04017050. https://doi.org/10.1061/(ASCE)WR.1943-5452.0000805.

Page, P. R., and E. Creaco. 2019. "Comparison of flow-dependent controllers for remote real-time pressure control in a water distribution system with stochastic consumption." *Water* 11 (3): 422. https://doi.org/10.3390/w11030422.

Page, P. R., S. Zulu, and M. L. Mothetha. 2018. "Remote real-time pressure control via a variable speed pump in a specific water distribution system." *J. Water Supply Res. Technol. AQUA* 68 (1): 20–28. https://doi.org/10.2166/aqua.2018.074.

Phillips, C. L., and R. D. Harbor. 2000. *Feedback control systems*. 4th ed. Upper Saddle River, NJ: Prentice-Hall.

Prescott, S. L., and B. Ulanicki. 2003. "Dynamic modeling of pressure reducing valves." *J. Hydraul. Eng.* 129 (10): 804–812. https://doi.org/10.1061/(ASCE)0733-9429(2003)129:10(804).

Prescott, S. L., and B. Ulanicki. 2008. "Improved control of pressure reducing valves in water distribution networks." *J. Hydraul. Eng.* 134 (1): 56–65. https://doi.org/10.1061/(ASCE)0733-9429(2008)134:1(56).

Rezaei, H., B. Ryan, and I. Stoianov. 2015. "Pipe failure analysis and impact of dynamic hydraulic conditions in water supply networks." *Procedia Eng.* 119: 253–262. https://doi.org/10.1016/j.proeng.2015.08.883.

Sigurd Skogestad, C. G. 2018. "Should we forget the Smith Predictor?" In Vol. 51 of *Proc., 3rd IFAC Conf. on Advances in Proportional-Integral-Derivative Control PID 2018*, 769–774. Ghent, Belgium: IFAC-PapersOnLine. https://doi.org/10.1016/j.ifacol.2018.06.203.

Strogatz, S. 2007. *Nonlinear dynamics and chaos: Studies in nonlinearity.* 1st ed. Boca Raton, FL: CRC Press.
Thornton, J., and A. Lambert. 2010. "Managing pressures to reduce new breaks." Accessed August 20, 2020. https://www.researchgate.net/publication/292685069_Managing_pressures_to_reduce_new_breaks.
Vande Vegte, J. 1986. *Feedback control systems*. 3rd revised ed. New York: Prentice Hall.
van Zyl, J. E., and A. M. Cassa. 2014. "Modeling elastically deforming leaks in water distribution pipes." *J. Hydraul. Eng.* 140 (2): 182–189. https://doi.org/10.1061/(ASCE)HY.1943-7900.0000813.
Vicente, D. J., L. Garrote, R. Sánchez, and D. Santillán. 2016. "Pressure management in water distribution systems: Current status, proposals, and future trends." *J. Water Resour. Plann. Manage.* 142 (2): 04015061. https://doi.org/10.1061/(ASCE)WR.1943-5452.0000589.